RDR 2026-011

Research Data & Reports

Volume 2, Issue 1 (2026)

Journal homepage: https://researchdr.in

Implications of time-dependent tensile response in the design of concrete tunnel segments with hybrid reinforcement

Stefie J. Stephen[1*] and Ravindra Gettu[2]

[1]*PhD Graduate, Department of Civil Engineering, Indian Institute of Technology Madras, Chennai, India, E mail: stefie.j.s@gmail.com*

[2]*V.S. Raju Chair Professor, Department of Civil Engineering, Indian Institute of Technology Madras, Chennai, India, E mail: gettu@iitm.ac.in*

** Corresponding author*

A B S T R A C T

The addition of fibres in concrete improves the mechanical performance of tunnel segment by bridging the crack, during construction and service stage. The approach normally used in design is the *P-M* interaction diagram, which is obtained primarily from the compressive and tensile response of the fibre reinforced concrete. Under service, the segments are subjected to prolonged static and dynamic loading, which could diminish the material performance. The aim of this paper is to investigate the influence of time-dependent loading on the mechanical behaviour of precast concrete tunnel segments reinforced with both steel fibres and rebars. Numerical analyses demonstrate the rate-sensitivity on the flexural performance of tunnel segment, which varies with the type and dosage of fibres. A fracture-based analytical design procedure to determine the capacities of the hybrid fibre reinforced concrete segment is modified to obtain time-dependent *P-M* diagrams. The results, both numerical and analytical, reveal a positive impact due to the incorporation of higher dosage of steel fibres in the segmental linings by the mitigation of loading-rate effects.

Keywords: *Tunnel segment; fracture-based design; fibre reinforced concrete; time-dependent effects.*

1 Introduction

Precast concrete segments offer permanent support for tunnels excavated using the tunnel boring machine (TBM), with conventional steel bars (rebars) normally being provided as reinforcement. Considering the high initial cost and complications associated with shutdowns for repair, such tunnel linings are expected to last for at least 100 years, if not more. However, cracking and spalling of concrete due to improper grouting, vibrations due to traffic, prolonged high overburden pressure, etc. puts the segments in jeopardy in the long run (Inokuma and Inano, 1996; Asakura and Kojima, 2003; Arnau et al., 2012). This may lead to reduction in the overall bearing capacity and durability, and could affect the normal operation of tunnels (Zhang et al., 2017).

In many cases, fibres or combinations (hybrid) of rebars and fibre reinforcement have been used in order to withstand the bursting and spalling stresses developed during the production, transportation and placement of precast segments (Caratelli et al., 2011). The fibres are also found to exhibit improve the shrinkage, fatigue and impact resistance of the concrete system (Briffaut et al., 2016). The role of the fibres is expected to dominate the design, especially if appropriate material and structural models are developed and used. The compressive and tensile strengths of concrete, and post-crack residual strength (or toughness) are the primary design parameters for fibre reinforced concrete (FRC) tunnel segments (Plizzari and Cominoli, 2005; Sorelli and Toutlemonde, 2005). A typical tensile stress-strain curve to represent the strain-hardening response of FRC could be of the form shown in Figure 1(a). This considers an initial linear elastic region until the tensile strength (ft) is reached, after which the fibres bridge the crack (beyond σ_1,w_1) and the tensile curve flattens or rises (beyond σ_2,w_2 and σ_3,w_3) depending upon the dosage and type of fibres (Barragán et al., 2003; Stephen et al., 2019). The uniaxial compressive stress-strain curve for FRC (Ding and Kusterle, 2000), which would also be required for the analysis, is relatively simple, as shown in Figure 1(b). Initially, there is a linear elastic regime followed by some pre-peak nonlinearity, and after the peak, the concrete softens and there is a progressive decrease in the axial stress with an increase in strain. These models can be given directly as input for the finite element models to assess the structural performance.

Though finite element analysis could be used, it is more common to design tunnel segments for service conditions using the capacity curve represented by the *P-M* interaction diagram, where *P* is the combined axial force and *M* is the bending moment. Such interaction diagrams for reinforced concrete are based on a rectangular stress block in the compression zone and concentrated forces at the steel reinforcement (Whitney and Cohent, 1956; Bresler, 1960; Rotter, 1983; Hernández-Montes et al., 2005), and the tensile capacity of the concrete is ignored. However, in the case of FRC, the tensile load-carrying capacity should be included in the design to consider the significant residual strength at both serviceability limit state (SLS) and ultimate limit state (ULS) (RILEM TC 162-TDF, 2003; CNR DT 204, 2006; fib Model, 2010). Table 1 summarises the different compression and tensile models used for the design of tunnel segments with FRC and hybrid reinforcement consisting of conventional rebars and fibres (HRC). Some researchers

https://doi.org/ 10.70002/iitm.rdr.1.1.50

Received on 23 March 2026, Accepted on 30 April 2026, Available online 17 May 2026

Publisher: Centre of Excellence (CoE) on Technologies for Low Carbon and Lean Construction (TLC2) at Indian Institute of Technology Madras

have obtained the *P-M* interaction diagram by representing the FRC response with a simplified rigid-plastic tensile stress-strain curve, for segments with fibres as sole reinforcement (Nanakorn and Horii, 1996; Caratelli et al., 2012; ACI 544.7R, 2016; Di Carlo et al., 2016) and for segments containing hybrid reinforcement (Liao et al., 2016). Other researchers have used softening tensile stress-strain curves for FRC (Chiaia et al., 2009; de la Fuente et al., 2012). Recently, Yao et al. (2018) represented the softening curve with an elastic + drop-constant model to construct the *P-M* diagram, using closed-formed analytical solutions, and obtained results that matched those from finite element analysis by de la Fuente et al. (2012). The procedure used by Yao et al. (2018) is used here because of its straightforward algorithm that can be modified and integrated into design procedures. In order to account for the time-dependence of the FRC response (Zhang et al., 2014; Stephen and Gettu, 2019, 2020), the present paper addressed this phenomenon to improve on the design. The incorporation of the effects of loading rate and fatigue on the structural response is illustrated here for tunnel segments reinforced with different types and dosages of fibres.

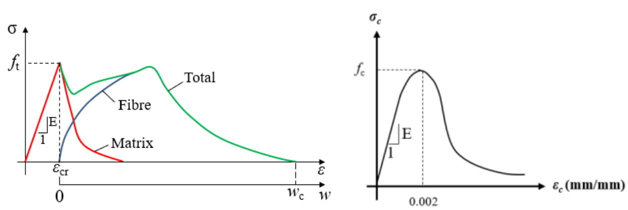

Figure 1 Response of FRC under uniaxial a) tension and b) compression

2 Analysis and design of tunnel segments

The constitutive models for the compressive and tensile responses of the FRC can be introduced in a finite element code to assess the behaviour of the tunnel lining. To illustrate the efficacy of the analysis, segments of the Barcelona Metro Line 9 tunnel lining, reinforced with both steel fibres and rebars are considered. The tunnel has a diameter of 12 m, and each 1.8 m wide ring is made of 7 full segments and one half-length key segment, all with thickness of 350 mm. The finite element programme TNO DIANA v9 is used for the analysis, and the cross-section of the reinforced FRC segment is modelled in 2-dimensions with solid tetrahedral elements of 50 mm size (Figure 2).

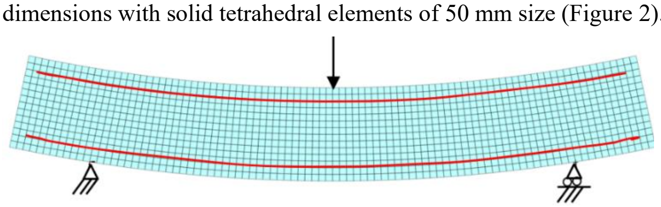

Figure 2 Finite element model of tunnel lining segment used for numerical analysis

The input for the constitutive model for FRC in tension (Figure 3a) is determined by inverse analysis of experimentally-obtained load-displacement curves corresponding to FRC with 30 kg/m3 of steel fibres (Gettu et al., 2004) with the strain taken as the crack width divided by the element size (i.e., crack opening/50) for each stress value; the constitutive model for compression is taken from IIT Madras test data on similar concrete (Figure 3b). The steel bar reinforcement of 8 mm diameter is modelled as 1D elements, with yield strength of 415 MPa and Young's modulus of 200 GPa. For the simply supported tunnel segment with load applied at mid-span, the response obtained from the present numerical analysis is compared with the experimental data in Figure 3c. It is seen that there is good agreement between the results obtained here with the 2D model and the experimental data (Gettu et al., 2004). It can, therefore, be concluded that the models of the types considered here can yield a good representation of the structural response of tunnel segments.

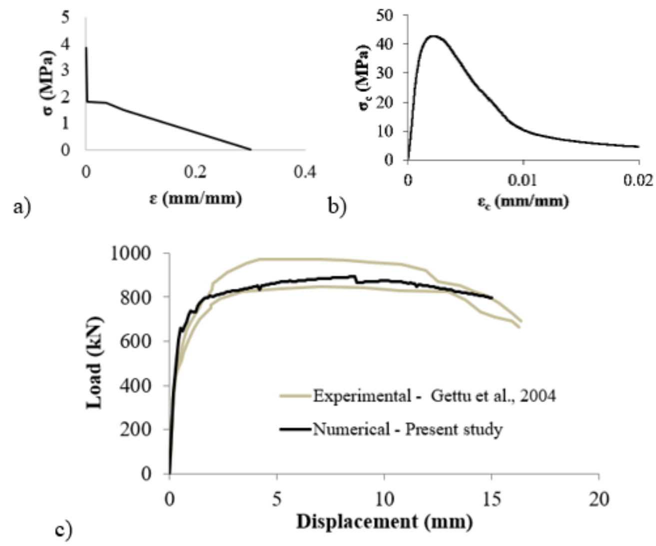

Figure 3 a) FRC tensile model obtained from inverse analysis, b) FRC compressive model, and c) flexural load carrying capacity of Barcelona tunnel segment

The approach used for the *P-M* interaction diagrams is briefly explained in the following paragraphs. The behaviour of FRC is simulated by the stress and strain diagrams for tension and compression that can be found in Table 1, and the response of the steel rebars is simulated using Figure 4. The following assumptions were adopted by Yao et al. (2018) for the development of the closed-formed design formulation:

- The tension model consists of a linear elastic stress-strain diagram until the stress reaches the tensile strength (ft) of the material and the strain at this point is termed as cracking strain ($\varepsilon cr = ft / E$). This is followed by a constant post-cracking residual tensile stress, $\sigma p = \mu ft = \mu E \varepsilon cr$, where parameter μ ($0 \leq \mu < 1$) is a fraction of the tensile strength. For plain concrete, μ is assumed to be 0 and for FRC, μ is assumed based on fibre dosage. The parameters of the tensile model are obtained from the flexural test response of beams, as per RILEM TC 162-TDF (2003).
- The compressive behaviour is simulated as an elastic perfectly plastic model, with a linear stress-strain diagram up to the yield compressive strength fc. Beyond the yield strain (0.2%), the stress is constant until concrete crushing ($\varepsilon c = \varepsilon cu$). The ultimate compressive strain, εcu, is assumed to be 0.35% (RILEM TC 162-TDF, 2003). The normalized yield compressive strength, ω, is the compressive-tensile strength ratio.
- For steel rebars, the tensile model is assumed as elastic perfectly-plastic, with a linear stress-strain diagram up to the yield strength of rebar, $fsy = \kappa f_t$, where, κ is the normalized yield strength, which is the ratio between the yield strength of steel rebar and the tensile strength of concrete. The yield strain of steel is taken as, $\varepsilon sy = fsyEs$, where *Es* is the Young's modulus of steel. Beyond the yield strain, the stress is constant until the strain reaches the elongation limit.

Table 1 Summary of the different models used by various investigators to determine the interaction diagram for FRC and HRC

Investigator	**Type of concrete**		**Analysis procedure**		**Compression model**	**Tension model**
	FRC	HRC	Analytical	Numerical		
Nanakorn and Horii (1996)	●		●		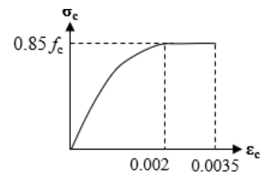 Nonlinear	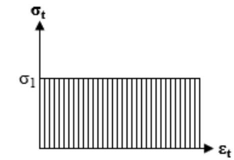 Rigid plastic
Caratelli et al. (2012); Di Carlo et al. (2016)	●		●		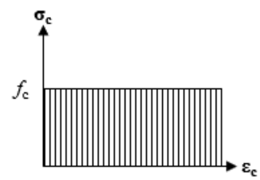	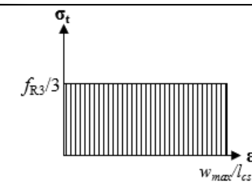 Rigid plastic model (fib Model, 2010)
Chiaia et al. (2009); de la Fuente et al. (2012)		●		●	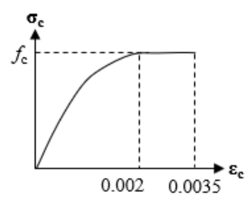 (RILEM TC 162-TDF, 2003)	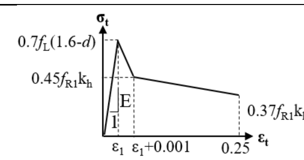 $k_h = 1.0 - 0.6\frac{h(cm) - 12.5}{47.5}$ (RILEM TC 162-TDF, 2003)
Bakhshi and Nasri (2014); ACI 544.7R (2016)	●		●		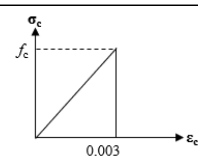	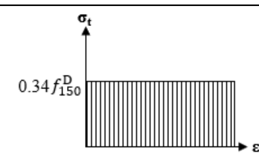
PAS 8810 (2016)		●		●	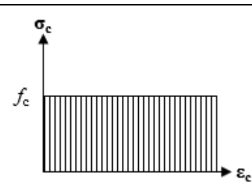	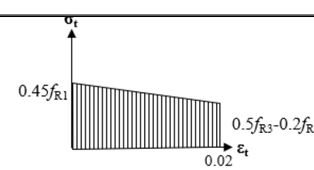 Linear model (fib Model, 2010)
Liao et al. (2016)		●		●	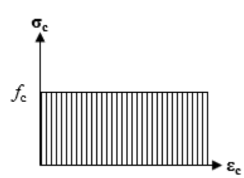	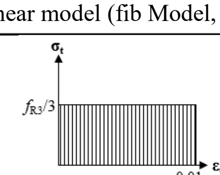 Rigid plastic model (fib Model, 2010)
Yao et al. (2018)		●	●		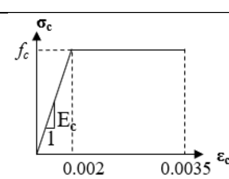 (RILEM TC 162-TDF, 2003)	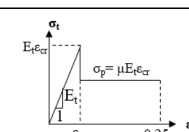 μ depends on the post-peak flexural response.

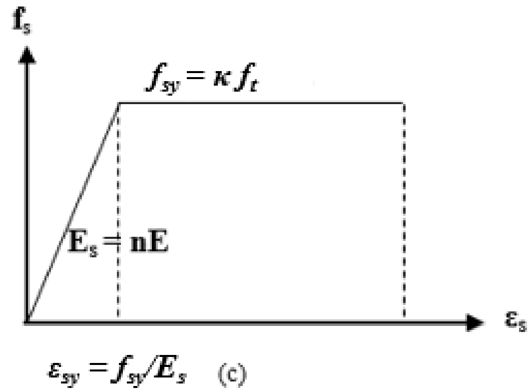

Figure 4 Material model for steel bars in tension (Yao et al., 2018)

The development of different phases of cracking (see Figure 5) are denoted as follows (Yao et al., 2018): Point A – pure compression, Point B – tensile stresses are developed, Point C – tensile cracking, Point D – yielding of steel rebar. The region between C and D is fully dominated by the fibres and beyond D, the steel rebars along with the fibres mitigate the tensile crack propagation. Based on the above-mentioned models and assumptions, the moment and axial force capacity of the tunnel segment of known dimensions can be calculated for different strain profiles. If the forces and moments due to the groundwater and soil loads are within the envelope of the developed interaction diagram, then the design is considered to be safe.

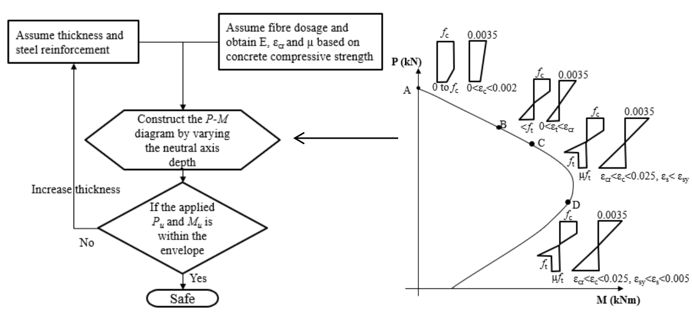

Figure 5 Procedure for the design of a concrete tunnel segment with hybrid reinforcement

The modifications and protocol proposed in this work to be used in the design are as follows:

- Uniaxial compressive testing of FRC cylinders and flexural testing of FRC beams are performed prior to the design of segment. The compression model for the present work is based on uniaxial compressive test results and the tension model is derived from the inverse analysis of flexural test results of beams.
- The tetralinear tensile stress-crack opening curve derived from inverse analysis of flexural test data (Stephen et al., 2019) is converted into bilinear curve, by considering plastic behaviour until the maximum allowable crack width. For ULS, the maximum crack width can be taken as 2.5 mm as per fib Model Code (2010). The stress-crack opening curve can be converted into the stress-strain curve by dividing crack opening, *w*, by the characteristic length, l_{cs}.
- The characteristic values (mean – *ks*, where k = 2.18 for 6 test samples) as per RILEM TC 162-TDF, 2003 are used for the tension models to account for the inherent variability in the FRC test results.
- Further, a strength reduction factor of 0.7, as per ACI 544.7R (2016), is used as the sections are subjected to compression and flexure.

Examples of *P-M* diagrams for the segments of the Barcelona Metro Line 9 tunnel lining (Gettu et al., 2004), reinforced with both steel fibres and rebars, are shown in Figure 6, for FRC belonging to fib '1.5b' and '5e' classes (Refer Clause 5.6.3 of fib Model (2010)). These two types of concrete satisfy the criteria required for ultimate limit state design. The tensile properties of the FRC is obtained by inverse analysis of flexural test data (published in Stephen and Gettu (2019)) and then converting the derived tetralinear tensile curve into the bilinear model; the consequent parameters are listed in Table 1. Note that the notation used for the different cases indicates the strength of the concrete, type of fibre incorporated (SF - steel fibre), its dosage in kg/m^3; e.g., M40SF45 denotes the 40 MPa characteristic strength, with 45 kg/m^3 of steel fibres. The inclusion of fibres seems to dominate the P-M diagram at higher bending strains; hence, the paper will focus on this regime of the curve in further discussions.

Table 1 Tensile property of fibre reinforced concrete

Concrete	*Class*	f_t (MPa)	σ_p (MPa)	f_{tk} (MPa)	σ_{pk} (MPa)
M40SF10	1.5b	3.10±0.35	0.66±0.07	2.33	0.50
M40SF45	5e	3.55±0.39	2.00±0.34	2.70	1.26

3 Rate-dependence of the tensile constitutive model

The tunnel segments under service must withstand slow soil settlement and groundwater movement. Even though these structural elements are designed for the magnitude of such loads, the variation of moment-carrying capacity with loading rate is not generally considered in the analysis or design. So, models accounting for the influence of loading rate on the tensile strength and residual bridging strength should be incorporated in the design appropriately. Based on tests covering 5 orders of magnitude of crack opening rate (Stephen and Gettu, 2019), the influence of rate in the *σ-w* curves has been modelled previously as:

$$f_{t,x} = f_{t,std} + m \log_{10}(\dot{\mathrm{CTOD}}_x) \quad (1)$$

where, $f_{t,x}$= tensile strength of concrete at the CTOD rate of $\dot{\mathrm{CTOD}}_x$ and $f_{t,std}$= tensile strength of concrete at the standard loading rate. For the present data, linear regression yields m = 0.46 MPa.s/μm for 1.5b class concrete, and m = 0.18 MPa.s/μm for 5e class concrete.

The rate-dependence of bridging stresses with cracking rate was found to be independent of the fibre type and dosage. Consequently, the rate-dependence of the bridging stress could be decoupled in terms of components corresponding to the tensile strength of the matrix (i.e., plain concrete) and the fibre bridging, as:

$$(\sigma_{i,x} - \sigma_{i,std}) = (f_{t,conc,x} - f_{t,conc,std}) + c\, log_{10}(\dot{\mathrm{CTOD}}_x), \text{ where } i = 1,2,3 \quad (2)$$

where c is a constant considered to be independent of the fibre dosage (-0.39 MPa.s/μm), and $f_{t,conc,x}$ and $\sigma_{i,x}$ are the tensile strength of the plain concrete and the bridging stress at the CTOD rate of $\dot{\mathrm{CTOD}}_x$, respectively. The Eqns. (1) and (2) comprise the model for rate-dependence of the fracture of FRC that shall be used in the modification of tensile constitutive relation.

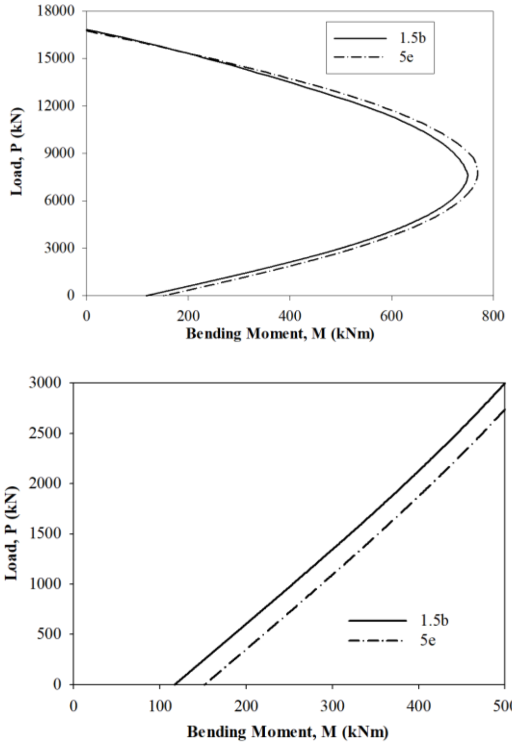

Figure 6 P-M diagram for the Barcelona tunnel segment with different dosages of fibres

3.1 Effect of loading rate on the flexural load carrying capacity

Numerical analysis can incorporate the modified tensile and the compressive material models yielding the responses shown in Figure 7 for the load carrying capacity of the segment at different loading rates, considering the crack opening rates of 0.01 and 100 μm/s. It can be seen that, when the loading rate decreases by 5 orders of magnitude, the cracking load decreases by about 45% for 'class 1.5b' and 20% for 'class 5e' concrete. Over a similar variation in loading, the capacity after further crack propagation, say at 2 mm deflection, decreases by about 15% for the 'class 1.5b' concrete, and 10% for concrete with higher toughness. It is evident that the effect of loading rate on the response of the tunnel segment is mitigated by the incorporation of higher dosages of steel fibres.

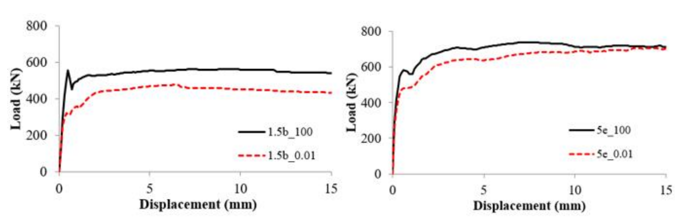

Figure 7 Effect of loading rate on the capacity of the tunnel segment with different dosages of steel fibre

3.2 Effect of loading rate on the *P-M* diagram

The rate-effect model is utilized to determine the time-dependent fracture properties required to derive the interaction diagram for the Barcelona tunnel segment (Figure 8). It is found that concrete with polymer fibre (PF) and the lowest dosage of steel fibre (SF) have greater rate-sensitivity in the segment moment carrying capacity. For instance, at zero axial force, the capacity reduces by 40% for 'class 1.5b' concrete and less than 20% for 'class 5e', as the loading rate reduces from 100 μm/s to 0.01 μm/s. So, for a tunnel segment reinforced with low dosage of steel fibres, it appears mandatory to include rate effects in the derivation of the interaction diagram.

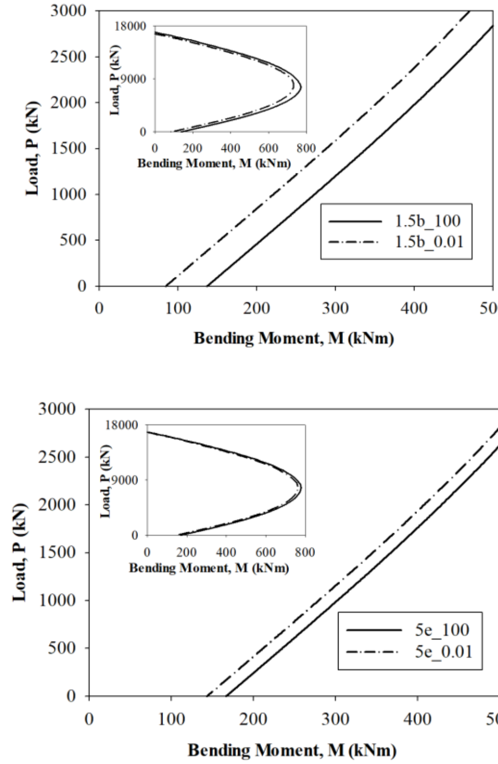

Figure 8 Loading rate effect on moment-force interaction diagram

4 Design incorporating post-crack fatigue models

In addition to prolonged loading, some FRC structures are subjected to fatigue loading under service, which could be in the form of traffic movement, temperature variation, wind action, etc. Fatigue reduction factors *X* and *Y* can be derived using the pre-peak and post-peak fatigue model, respectively, as illustrated in Figure 9, and the corresponding pre-peak and post-peak strength parameters that are involved in the design can be modified (as proposed by Nayar and Gettu, 2020).

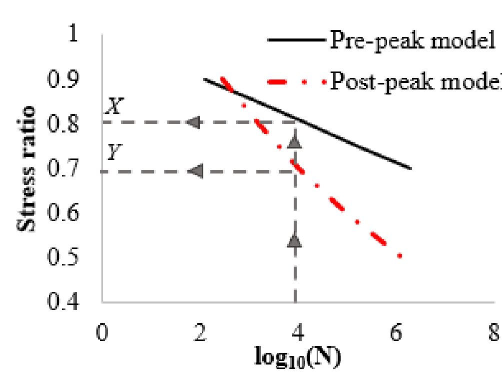

Figure 9 Fatigue reduction factors derived from S-N curves

In this approach, *X* is used as the reduction factor for the tensile strength of concrete (Xf_t) and *Y* is used as the reduction factor for the bridging strength ($Y\sigma_p$). Since the pre-peak fatigue performance has been studied extensively by various researchers, the S-N model suggested in the literature such as that of IRC SP:46 (2013) for FRC can be used. In the case of post-peak fatigue, a model based on critical CMOD, developed by Stephen and Gettu (2020), for FRC with different dosages of steel fibres, is applied. The values of the reduction factor for FRC reinforced with different dosage of steel fibres, which will be used in the design procedure, are listed in Table 2.

Table 2 The values of the fatigue reduction factors for desired fatigue life for FRC with different dosages of steel fibres

N	X		Y	
	1.5b	5e	1.5b	5e
1000	0.75	0.86	0.88	1.00
10,000	0.67	0.81	0.74	0.82
1,00,000	0.59	0.76	0.63	0.63
20,00,000	0.50	0.70	0.48	0.50

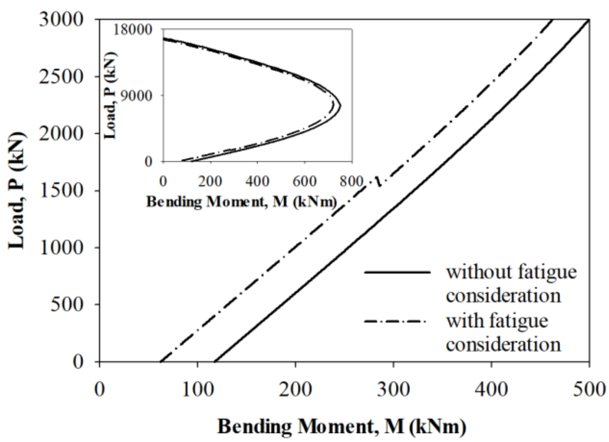

a) Class 1.5b

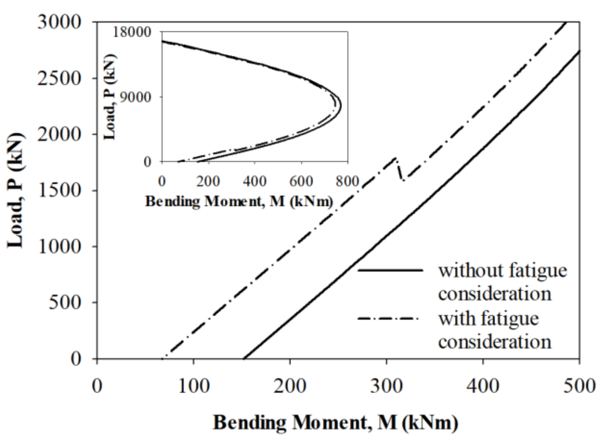

b) Class 5e

Figure 10 Variation of moment-force interaction diagram of tunnel segment with and without the consideration of fatigue

In previous work (Stephen and Gettu (2020)), the fatigue resistance at very large strains was shown to be negligible and hence, the reduction factor Y is taken to be zero for strains greater than 0.025 (i.e., crack opening = 1.25 mm), and the interaction diagram at different fatigue cycles is consequently obtained (Figure 10). The kink observed in the diagram is because of the drop-constant model and zeroing of the bridging strength at larger strain. At zero axial force, the moment carrying capacity of the FRC segment considering fatigue loading over 2 million cycles is about 35% and 45% lower than that without considering fatigue loading, for segments made of 10 kg/m^3 and 45 kg/m^3 of steel fibres, respectively. It appears that the inclusion of fatigue-based design is more crucial when the segment is subjected to proportionally higher bending strain.

5 Conclusions

In this paper, a design methodology to incorporate time-dependent fracture properties of fibre reinforced concrete has been proposed. The significance of the methodology is discussed in terms of the variation of the section capacity with loading rate and fatigue loading. The design of hybrid tunnel segments, which utilise toughness as a design input, is chosen to illustrate the proposed procedure, with appropriate modification factors obtained from rate effect and fatigue models. Further,

- The load carrying capacity of tunnel segment was investigated at different loading rates by means of numerical simulation and was found to decrease with lower loading rate. The segments reinforced with low dosage of steel fibres are significantly affected by long-term loading, though the increase in steel fibre dosage or steel rebars mitigates such effects. Therefore, it is important to consider rate effect models for tunnel segments, especially if FRC of low toughness is used.
- The influence of fatigue loading on the moment carrying capacity of the tunnel segment under service was studied and found to be increase significantly when there is pure bending. It is evident that fatigue-based design is more crucial when the segment is subjected to proportionally higher bending.

References

[1] ACI 544.7R, 2016. Report on design and construction of fiber-reinforced precast concrete tunnel segments. American Concrete Institute. Farmington Hills, MI.

[2] Arnau, O., Molins, C., Blom, C.B.M., Walraven, J.C., 2012. Longitudinal time-dependent response of segmental tunnel linings. Tunn. Undergr. Sp. Technol. 28, 98–108. https://doi.org/10.1016/j.tust.2011.10.002

[3] Asakura, T., Kojima, Y., 2003. Tunnel maintenance in Japan. Tunn. Undergr. Sp. Technol. 18, 161–169. https://doi.org/10.1016/S0886-7798(03)00024-5

[4] Bakhshi, M., Nasri, V., 2014. Developments in design for fibre-reinforced concrete tunnel segments. Am. Concr. Institute, ACI Spec. Publ. 2014-July, 341–352. https://doi.org/10.35789/fib.bull.0079.ch33

[5] Barragán, B.E., Gettu, R., Martín, M.A., Zerbino, R.L., 2003. Uniaxial tension test for steel fibre reinforced concrete—a parametric study. Cem. Concr. Compos. 25, 767–777. https://doi.org/http://dx.doi.org/10.1016/S0958-9465(02)00096-3

[6] Bresler, B., 1960. Design criteria for reinforced columns under axial load and biaxial bending. J. Am. Concr. Inst. 10, 481–490.

[7] Briffaut, M., Benboudjema, F., D'Aloia, L., 2016. Effect of fibres on early age cracking of concrete tunnel lining. Part II: Numerical simulations. Tunn. Undergr. Sp. Technol. 59, 221–229. https://doi.org/10.1016/j.tust.2016.08.001

[8] Buratti, N., Ferracuti, B., Savoia, M., 2013. Concrete crack reduction in tunnel linings by steel fibre-reinforced concretes. Constr. Build. Mater. 44, 249–259. https://doi.org/10.1016/j.conbuildmat.2013.02.063

[9] Caratelli, A., Meda, A., Rinaldi, Z., 2012. Design according to MC2010 of a fibre-reinforced concrete tunnel in Monte Lirio, Panama. Struct. Concr.

13, 166–173. https://doi.org/10.1002/suco.201100034
[10] Caratelli, A., Meda, A., Rinaldi, Z., Romualdi, P., 2011. Structural behaviour of precast tunnel segments in fiber reinforced concrete. Tunn. Undergr. Sp. Technol. 26, 284–291. https://doi.org/10.1016/j.tust.2010.10.003
[11] Chiaia, B., Fantilli, A.P., Vallini, P., 2009. Combining fiber-reinforced concrete with traditional reinforcement in tunnel linings. Eng. Struct. 31, 1600–1606. https://doi.org/10.1016/j.engstruct.2009.02.037
[12] CNR DT 204, 2006. Guidelines for the design, construction and production control of fibre reinforced concrete structures. National Research Council of Italy.
[13] de la Fuente, A., Pujadas, P., Blanco, A., Aguado, A., 2012. Experiences in Barcelona with the use of fibres in segmental linings. Tunn. Undergr. Sp. Technol. 27, 60–71. https://doi.org/10.1016/j.tust.2011.07.001
[14] Di Carlo, F., Meda, A., Rinaldi, Z., 2016. Design procedure for precast fibre-reinforced concrete segments in tunnel lining construction. Struct. Concr. 17, 747–759. https://doi.org/10.1002/suco.201500194
[15] Ding, Y., Kusterle, W., 2000. Compressive stress-strain relationship of steel fibre-reinforced concrete at early age. Cem. Concr. Res. 30, 1573–1579. https://doi.org/10.1016/S0008-8846(00)00348-3
[16] fib Model, 2010. Code for Concrete Structures. fib CEB-FIP publication.
[17] Gettu, R., Barragán, B., García, T., Fernández, C., Oliver, R., 2004. Steel fiber reinforced concrete for the Barcelona metro line 9 tunnel lining. 6th Int. RILEM Symp. Fibre Reinf. Concr. 141–156.
[18] Hernández-Montes, E., Gil-Martín, L.M., Aschheim, M., 2005. Design of concrete members subjected to uniaxial bending and compression using reinforcement sizing diagrams. ACI Struct. J. 102, 150–158. https://doi.org/10.14359/13540
[19] Inokuma, A., Inano, S., 1996. Road tunnels in Japan: Deterioration and countermeasures. Tunn. Undergr. Sp. Technol. 11, 305–309. https://doi.org/10.1016/0886-7798(96)00026-0
[20] IRC:SP:46, 2013. Guidelines for design and construction of fibre reinforced concrete pavements. Indian road congress, New Delhi.
[21] Liao, L., de la Fuente, A., Cavalaro, S., Aguado, A., 2016. Design procedure and experimental study on fibre reinforced concrete segmental rings for vertical shafts. Mater. Des. 92, 590–601. https://doi.org/10.1016/j.matdes.2015.12.061
[22] Nanakorn, P., Horii, H., 1996. A fracture-mechanics-based design method for SFRC tunnel linings. Tunn. Undergr. Sp. Technol. 11, 39–43. https://doi.org/10.2208/jscej.1996.532_221
[23] PAS 8810, 2016. Tunnel design - Design of concrete segmental tunnel linings.
[24] Plizzari, G.A., Cominoli, L., 2005. Numerical simulations of SFRC precast tunnel segments, in: Erdem, Y., Solak, T. (Eds.), In Proceedings of ITA-AITES 2005, Underground Space Use: Analysis of the Past and Lessons for the Future. Istanbul (Turkey), pp. 1105–1112.
[25] RILEM TC 162-TDF, 2003. Final recommendation of RILEM TC 162-TDF: Test and design methods for steel fibre reinforced concrete sigma-epsilon-design method. Mater. Struct. 36, 560–567. https://doi.org/10.1617/14007
[26] Rotter, J.M., 1983. Rapid exact inelastic biaxial bending analysis. J. Struct. Eng. 111, 2659–2674.
[27] Sorelli, L.G., Toutlemonde, F., 2005. On the Design of Steel Fibre Reinforced Concrete Tunnel Lining Segments. 11th Int. Conf. Fract. 3–8.
[28] Stephen, S.J., Gettu, R., 2020. Fatigue fracture of fibre reinforced concrete in flexure. Mater. Struct. 1–16.
[29] Stephen, S.J., Gettu, R., 2019. Rate-dependence of the tensile behaviour of fibre reinforced concrete in the quasi-static regime. Mater. Struct. 52, 107. https://doi.org/10.1617/s11527-019-1405-2
[30] Stephen, S.J., Raphael, B., Gettu, R., Jose, S., 2019. Determination of the tensile constitutive relations of fibre reinforced concrete using inverse analysis. Constr. Build. Mater. 195, 405–414.
[31] Whitney, B.C.S., Cohent, E., 1956. Guide for Ultimate Strength Design of Reinforced Concrete. ACI J. Proc. 53, 455–490. https://doi.org/10.14359/11524
[32] Yao, Y., Bakhshi, M., Nasri, V., Mobasher, B., 2018. Interaction diagrams for design of hybrid fiber-reinforced tunnel segments. Mater. Struct. 51, 1–17. https://doi.org/10.1617/s11527-018-1159-2
[33] Zhang, X.X., Abd Elazim, A.M., Ruiz, G., Yu, R.C., 2014. Fracture behaviour of steel fibre-reinforced concrete at a wide range of loading rates. Int. J. Impact Eng. 71, 89–96. https://doi.org/10.1016/j.ijimpeng.2014.04.009
[34] Zhang, Y., Shi, Y., Zhao, Y., Yang, J., 2017. Damage in Concrete Lining of an Operational Tunnel. J. Perform. Constr. Facil. 31. https://doi.org/10.1061/(ASCE)CF.1943-5509.0001032